21st Australasian Fluid Mechanics Conference
Adelaide, Australia
10-13 December 2018

Chamber Geometry Effect on Non-Evaporating Diesel Spray Evolution

D. Nguyen, D. Honnery

Department of Mechanical and Aerospace Engineering
Monash University, Melbourne, Victoria 3800, Australia

Abstract

The effect of spray chamber geometry on the penetration and spreading angle of common rail non-reacting diesel sprays at room temperature condition in a constant volume chamber has been investigated. The high pressure cylindrical chamber used has dimensions similar to those used in the literature. Spray chamber internal geometry was modified to yield five different chamber height-to-diameter ratios and two different nozzle stand-off distances. Sprays from a sing-hole nozzle were examined for an injection pressure of 1000bar into a chamber pressure of 50bar, which closely resemble the operating conditions in a number of real engines. A volume illumination method was used to characterise the spray structure that covers tip penetration, tip speed and spray spread angle. For pressure conditions used, little sensitivity to vessel geometry was found for variation in height to diameter ratio from 0.6 to 5.1 and variation in nozzle stand-off distance from 2mm to 54mm. While the spray spread angle was found to be very sensitive to the image intensity threshold value, the spray tip penetration remained very stable over the range of intensity threshold values investigated.

Introduction

To help better understand the combustion process in high pressure spray combustion applications such as diesel engines, we continue to study the spray itself. Parameters that can affect spray development, vaporization and consequently combustion include fuel properties, nozzle geometry, injection pressure, ambient pressure/temperature, ambient gas compositions and the combustion chamber geometry. Some groups have focused on the effect of injection pressure and/or ambient pressure/temperature [1−5], fuel properties [6], and ambient gas composition [3,4]. The development of x-ray based measurement techniques and silicone moulding, which enables mapping of the internal characteristics of nozzles, has also led to examination of the role of nozzle geometry (e.g. [5,7,8]). The role of spray chamber geometry, which has been studied to a far lesser extent, has been reported in a number of papers (e.g. [9,10]) for engines but not explicitly for spray research chambers.

An important aspect is the need for consistency in the methods, facilities and injectors used if the influence of the parametric space is to be fully understood. This is particularly important given the sensitivity of spray macroscopic properties to subtle differences in nozzle hole geometry and surface finish [7,8,11]. To this end, the engine combustion network (ECN) developed a series of nozzles to be tested in similar conditions by participating groups but using their individual facilities and techniques. Among the examples of this approach are the studies undertaken on the nozzle known as spray A [4,7,11]. Although ECN participants have generally reported consistency in such properties as penetration, ignition delay and flame lift-off length for combusting sprays for this nozzle, some differences remain in properties such as spray liquid length, with possible sources for these differences being methods used to image the sprays and to heat the chamber. Difference in the geometry of the spray chamber they used is another important factor and it is difficult to separate the role of this geometry in these results.

Given such a situation, an independent study into the role of chamber geometry on spray macroscopic properties using the same injector/nozzle, fuel, fuel supply system, and data processing methodology is needed. To address this, this work focuses on non-evaporating diesel sprays operating at typical engine pressure conditions. The reason for this is that non-evaporating sprays enable a higher number of repeat measurements than combusting sprays which require preheating, temperature stabilisation and post burn flushing. Large sample number is important as it allows for greater confidence when assessing the significance of any observed difference between test cases.

For this approach, a high pressure spray chamber has been developed with its internal shape being alterable by use of inserts. The inserts enable both diameter and height to be independently altered, so that the role of chamber geometry on spray tip penetration and velocity, and spray spreading angle can be explored. A single-hole nozzle is examined at a chamber pressure of 50bar and an injection pressure of 1000bar. All measurements are done with the same fuel, same imaging system and same data analysis methodology. Also included is a thorough investigation of sensitivity. For chamber geometries examined, little sensitivity to chamber geometry was found.

Methodology

Experimental Facility

The experiments were done in the Laboratory for Turbulence Research in Aerospace and Combustion (LTRAC). Components of the experimental system are similar to that in [1], but with a different constant volume chamber and different arrangement of illumination sources, see figure 1. This vessel has rectangular external shape with each of its four sides designed to allow for optical access through glass windows. The internal shape is cylindrical, measuring 100mm in diameter and 260mm in height along its centreline. With this height, the spray splash on the vessel bottom is minimized and the height adjustment is more flexible. The 100mm diameter design is similar to more recent facilities of other groups [4].

A Bosch common rail injector was located at the top of the steel vessel and driven by a solenoid driver. The injector was operated with a single-hole nozzle which directed the spray vertically down. The nozzle hole nominal diameter is 200μm which was produced via electro discharge machining with no additional finishing. Standard Australian automotive diesel was supplied at high pressure to the injector through a common rail from a feedback controlled pump which is able to maintain the pressure to within ±5bar of the set value. This pump received diesel from a primary pump connected to a temperature monitored fuel tank. Fuel returned to the tank from the common rail after passing through a heat exchanger. Fuel temperature was maintained in the range 30−32^{o}C. The same fuel was used for all experiments. Fuel density

(830kg/m^3) and viscosity (2.52mPa.s), monitored before and after the experiments, remained unchanged.

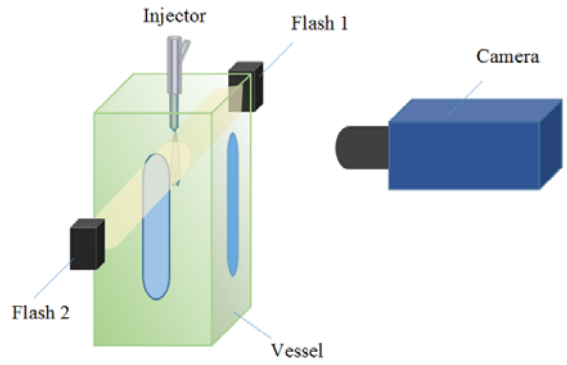

Figure 1. Sketch of system optical arrangement.

To record the spray development, a high speed HPV1 Shimadzu digital camera was used, which has a CCD array of 312×260px^2. The sprays were illuminated by two high power TTL Met−Mecablitz flash units (figure 1). For this setup, only three sides of the chamber were fitted with glass windows while one side was fitted with a metal blank. The trigger signals to the injector, flash units and camera were produced and co-ordinated by use of a signal generator and a custom made control box. Fitted to the camera was a micro Nikkon lens of 105mm. Image area was fixed to (WxH) ≈ 39.6×33mm^2 giving the spatial resolution of 7.87px/mm. For these measurements, the camera frame rate was set at 125kfps with a 1μs integration time. Lens focal length f-stop was set at 11 to record as the sprays propagated across the viewing area.

Chamber geometry was modified by use of a chamber height adapter (CHA) and acrylic tubes. While the CHA allowed for variation in spray chamber height, the acrylic tubes effectively modified chamber diameters. The CHA has upper and lower metal plates, which extend across the bore of the vessel. These plates are fixed by 4 steel posts on which they move to give variable height. The top plate has a central hole to allow the injector nozzle to pass through, while the bottom plate has a small hole to allow the escape of accumulated fuel to limit fuel splashing, thus reducing interference with the optical path. Figure 2 shows the dimensioned drawings which illustrate the five different geometrical cases used in this study. These configurations allowed the study of the effect of the distance between the nozzle tip and the upper surface (nozzle stand-off distance N_{sd}, which has been reported elsewhere to play some role on the spray development), the chamber height H (distance between the upper and lower surfaces), and the chamber diameter D.

Changes in both chamber diameter and height were made to cover a large range in height to diameter ratio, and to match height to diameter ratios between individual cases. Optical interference from fuel residue after repeat sprays limited the variations possible, particularly when using acrylic tubes. Case A is the unaltered chamber for which the height to diameter ratio H/D=2.6. For case A, nozzle stand-off distance is N_{sd}=54mm. Case B makes use of the upper plate of the CHA, which by locating it such that N_{sd}=2mm has H/D=2.08. For case C, a 234mm long acrylic tube was located in the chamber to reduce the diameter from 100mm to 51mm giving H/D=5.1, noting that maximum height of the chamber remains at 260mm for this condition. Case D is a chamber height of 105mm, with chamber diameter reduced to 51mm by a 105mm high acrylic tube giving H/D=2.06, and similar to case B with N_{sd}=2mm. To enrich the investigation, included is case E in which the two CHA plates were set to be only 60mm apart from each other giving H/D=0.6, and N_{sd}=2mm.

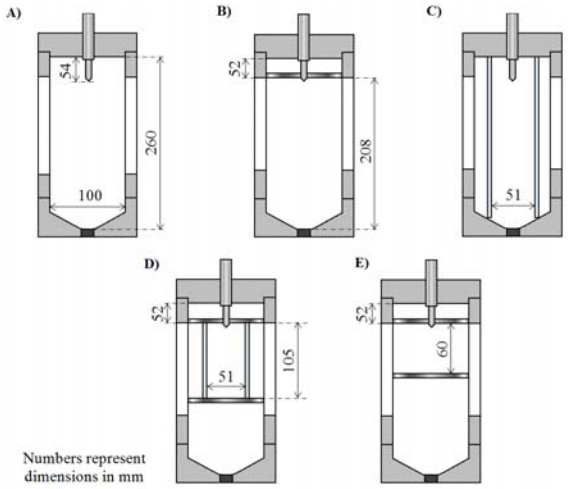

Figure 2. The five chamber geometries examined: A) case A is the unaltered chamber with H/D=2.6, N_{sd}=54mm; B) case B with H/D=2.08, N_{sd}=2mm; C) case C with H/D=5.1, N_{sd}=54mm; D) case D with H/D=2.06, N_{sd}=2mm; and E) case E with H/D=0.6, N_{sd}=2mm.

Image Analysis

The spray tip penetration length (*STPL*) is defined as the distance from the nozzle tip to the farthest part of the spray's leading edge. To find the location of the leading edge, the approach used in this work is based on a direct quadratic function fit to the intensity profile along a one-pixel-wide strip of the region surrounding the spray leading edge as has been described in [12]. This operation with the use of two threshold intensities (T1 for skipping image noise and T2 for defining the edge) is fast and sub-pixel accurate. Spray tip speed is given as the time rate change in average *STPL*. Time dependent average *STPL* is taken as the ensemble average of the individually acquired sprays.

Calculation of spray spread angle α as a function of time requires finding the width of the spray over much of its length. The spray width is greatly affected by turbulent mixing in the spray's shear layer which is often wrinkled and diffuse. In this paper, spray spread angle is defined as the angle subtended between two lines connecting the nozzle tip to each side of the spray given by the width located at a distance of 75% of the *SPTL*. Mean spray angle is calculated as the ensemble average of the angles of individual sprays.

Sensitivity test

As intensity thresholds are used to derive the measured quantities, sensitivity checks against these values are important. For each geometrical case, there were around 100 repeated measurements. Taking case C for illustration, figure 3a shows mean penetration data against time for a range of T2 threshold values bracketing the selected value 65 (T1 is always 5 values lower than T2). It can be seen from this figure that mean penetration length is not sensitive to this range of threshold values. Even at the maximum tip penetration length, the variation is insignificant with the sample standard deviation to be almost unchanged, figure 3b.

Sensitivity test for spread angle calculation is shown in figure 4a. Sensitivity to the threshold value was found evident, especially during the early injection phase which is deemed influenced by the leading edge vortex which dominates its tip. For the data in this figure, this is partly, but not fully,

eliminated by limiting the angle calculation to times past when this effect is the greatest.

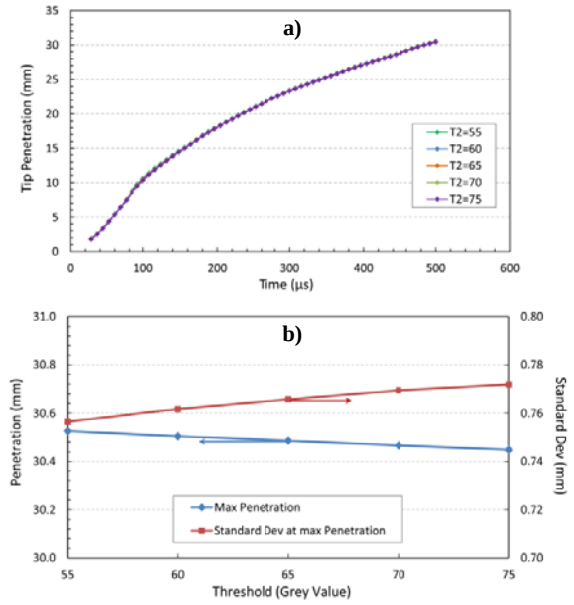

Figure 3. a) Mean penetration against time at different threshold T2 values; b) penetration and sample standard deviation at maximum penetration length against T2 values. Data shown for case C.

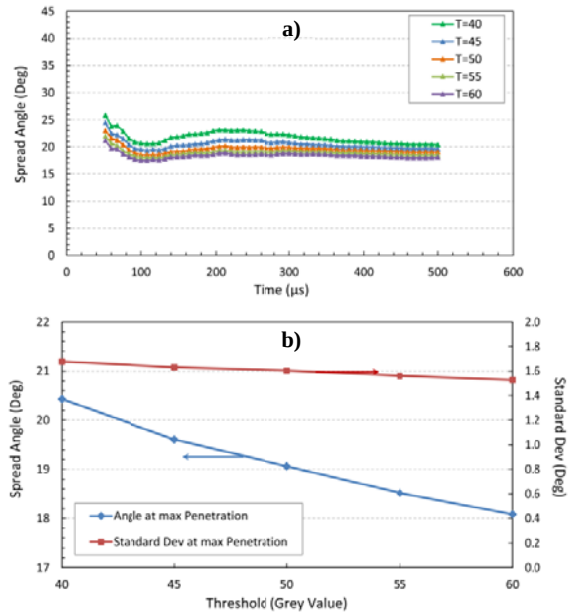

Figure 4. a) Mean spread angle against time at different threshold values; b) Mean spread angle and sample standard deviation at maximum penetration length against threshold values. Data shown for case C.

Variations in the mean spread angle and the sample standard deviation at the maximum penetration length with intensity threshold were found to be large (figure 4b). From this analysis, while tip penetration is robust to the variation in the intensity value used to locate the spray's leading edge, spread angle calculation is sensitive to this value although differences in the angles diminish with increasing spray duration.

Results

The nozzle used has a steady state discharge coefficient C_D≈0.657 (measured in atmospheric condition with same injection pressure of 1000bar). This low C_D suggests the possibility of cavitation in this nozzle. For all measurements, the injection pulse duration was set for 1ms. The spray chamber was filled with compressed air at room temperature. Figure 5 shows examples of spray images at 484µs after start of injection for five geometrical cases A-E. Only small differences in penetration are apparent among these cases which will be seen later to fall within the shot-to-shot variation found for this pressure condition. Some effect of the acrylic tube insert is evidenced by a slight blurring of the lower intensity resolution regions of the sprays for cases C and D. Image distortion occurring from use of these tubes was found to be almost negligible (< 0.15% of spray width).

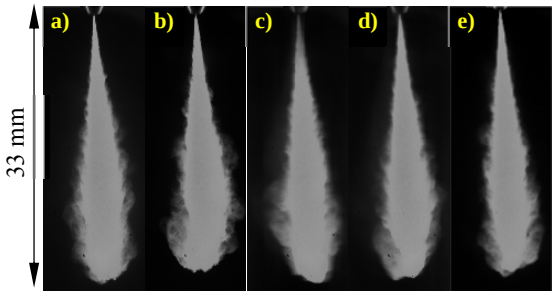

Figure 5. Examples of spray images taken from single events at 484µs for: a) case A; b) case B; c) case C; d) case D; e) case E.

Figure 6 presents mean penetration, tip speed and spray spread angle for all cases A-E. As can be seen in figure 6a, the penetration is almost similar for all cases. Typical variation in uncertainty at 95% confidence level in these measurements based purely on shot-to-shot variation is shown in figure 6a for case C as an example. Variation across the spray occurs because of the absolute limit in spatial resolution, and because of the increasing scale in the turbulence of the leading edge. Additional sources are the nozzle itself, particularly during the needle lift transient, and variation in fuel pressure [7]. For all cases, uncertainty ε is less than ±0.3mm (around ±1%) at maximum penetration. Differences in penetration fall within the bounds of the uncertainty ranges for the individual cases.

For tip speed (figure 6b), all cases show the typical initial rise to a peak, which for these sprays occurs at around 70µs, followed by a decay, following the same trends as shown in [1]. There are some differences amongst these cases, especially around the peak velocity, but these are typical of the variation found for this measurement [2]. Spray spread angle, figure 6c, presents the most variation among the measurements, particularly during the early stages. Differences in the final angle reached fall outside the uncertainty range for this measurement, which is shown in figure 6c to be typically less than around ε= ±0.6°. This suggests that measured differences are not a direct consequence of shot-to-shot variation and could therefore be linked to changes in chamber geometry. However, since these differences are not replicated in the penetration, it is likely they result from the measurement technique as discussed earlier. As noted, during the early stages, spread angle is sensitive to the initiation and passage of the leading edge vortex, while the ability to accurately resolve the spray trailing structure is limited by spatial resolution of the measurement. Similar uncertainty arises when attempting to determine the role of nozzle offset distance N_{sd}. Cases B, D and E have N_{sd}=2mm, while cases A and C have N_{sd}=54mm, yet the evolution of the spray spreading angle is similar for cases A, D and C, and for cases B and E.

It is notable that for pressure conditions which closely replicate that at the end of the compression stroke of some

diesel engines, the chamber geometries investigated have almost no effect on spray development. This shows that gas entrainment is playing a similar role in these study cases. In actual engines, however, factors related to piston movement and spray impingement can be expected to alter spray structure for different engine combustion chamber geometry.

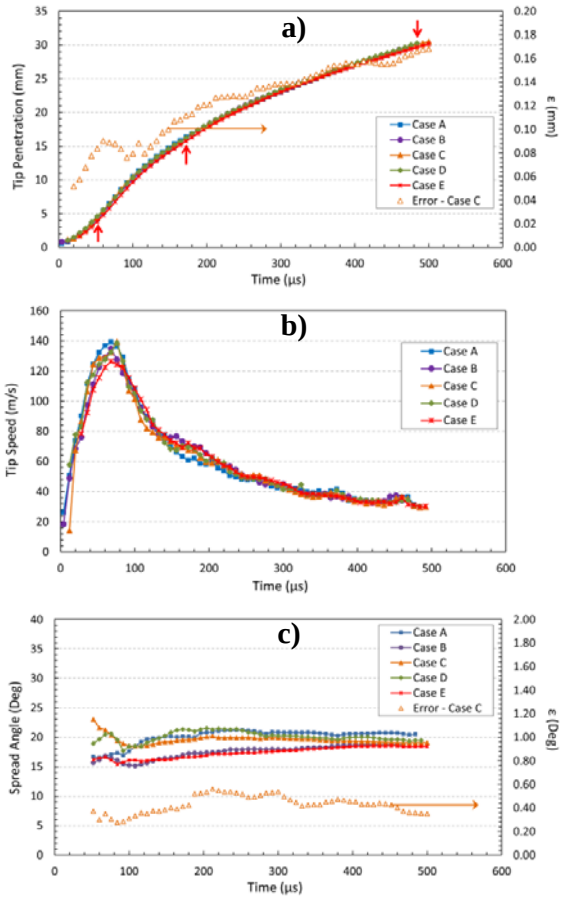

Figure 6. Cases A, B, C, D and E: a) Penetration and a typical distribution of experimental uncertainty; b) tip speed; and c) spread angle and a typical distribution of experimental uncertainty.

Conclusions

The effect of chamber geometry on the development of diesel sprays has been examined for a single-hole nozzle in pressure conditions similar to real engines. For an injection pressure of 1000bar and chamber pressure of 50bar, spray structure was found to be largely independent of variations in chamber height to diameter ratio ranging from 0.6 to 5.1. Little influence was observed in tip penetration for variation in nozzle stand-off distance when altered from 54 to 2mm. The tip penetration differences among geometrical cases studied were of the order of the measurement uncertainty. The spray spread angle was found to be sensitive to the image intensity threshold value used to define the edge of the spray; this is in contrast to the penetration calculation which shows very little sensitivity.

Acknowledgments

We would like to acknowledge the Australian Research Council for financial support of this project.

References

[1] Kostas, J., Honnery, D. & Soria, J., Time Resolved Measurements of the Initial Stages of Fuel Spray Penetration, *Fuel*, **88**, 2009, 2225−37.

[2] Kostas, J., Honnery, D. & Soria, J., A Correlation Image Velocimetry-Based Study of High-Pressure Fuel Spray Tip Evolution, *Exp. Fluid*, **51**, 2011, 667−78.

[3] Payri, F., Payri, R., Bardi, M. & Carreres, M., Engine Combustion Network: Influence of the Gas Properties on the Spray Penetration and Spreading Angle, *Exp. Therm. and Fluid Sci.*, **53**, 2014, 236−43.

[4] Meijer, M., Somers, B., Johnson, J., Naber, J., Lee, S.Y., Malbec, L.M., Bruneaux, G., Pickett, L.M., Bardi, M., Payri, R. & Bazyn, T., Engine Combustion Network (ECN): Characterisation and Comparison of Boundary Conditions for Different Combustion Vessels, *Atomization and Sprays*, **22** (9), 2012, 777−806.

[5] Du, C., Anderson, M. & Anderson, S., Effect of Nozzle Geometry on the Characteristics of an Evaporating Diesel Spray, *SAE Int. J. Fuels Lubr.*, **9** (3), 2016, DOI: 10.4271/2016−01−2197.

[6] Postrioti, L., Grimaldi, C.N., Ceccobello, M. & Di Gioia, R., Diesel Commonrail Injection System Behavior with Different Fuels, *SAE* Technical Paper No. 2004−01−0029, 2004.

[7] Kastengren, A.L., Tilocco, F.Z., Powell, C.F., Manin, J., Pickett, L.M., Payri, R. & Bazyn, T., Engine Combustion Network (ECN): Measurements of Nozzle Geometry and Hydraulic Behavior, *Atomization and Sprays*, **22** (12), 2012, 1011−52.

[8] Payri, F., Bermudez, V., Payri, R. & Salvador, F.J., The Influence of Cavitation on the Internal Flow and the Spray Characteristics in Diesel Injection Nozzles, *Fuel*, **83**, 2004, 419−31.

[9] Montajir, R.M., Tsunemoto, H., Ishitani, H. & Minami, T., Fuel Spray Behaviors in a Small DI Diesel Engine: Effect of Combustion Chamber Geometry, *SAE* Technical Paper No. 2000−01−0946, 2000.

[10] Jaichandar, S., Kumar, P.S. & Annamalai, K., Combined Effect of Injection Timing and Combustion Chamber Geometry on the Performance of a Biodiesel Fueled Diesel Engine. *Energy*, **47**, 2012, 388−94.

[11] Pei, Y., Davis, M.J., Pickett, L.M. & Som, S., Engine Combustion Network (ECN): Global Sensitivity Analysis of Spray A for Different Combustion Vessels, *Combustion and Flame*, **162**, 2015, 2337−47.

[12] Nguyen, D., Duke, D., Kastengren, A., Matusik, K., Swantek, A., Powell, C.F. & Honnery, D., Spray Flow Structure from Twin-hole Diesel Injector Nozzles, *Exp. Therm. and Fluid Sci.*, **86**, 2017, 235−47.